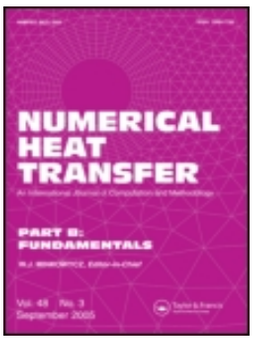

Numerical Heat Transfer, Part B Fundamentals

ISSN: 1040-7790 (Print) 1521-0626 (Online) Journal homepage: https://www.tandfonline.com/loi/unhb20

MODIFIED COLLOCATED SIMPLEC ALGORITHM APPLIED TO BUOYANCY-AFFECTED TURBULENT FLOW USING A MULTIGRID SOLUTION PROCEDURE

Peter Johansson & Lars Davidson

To cite this article: Peter Johansson & Lars Davidson (1995) MODIFIED COLLOCATED SIMPLEC ALGORITHM APPLIED TO BUOYANCY-AFFECTED TURBULENT FLOW USING A MULTIGRID SOLUTION PROCEDURE, Numerical Heat Transfer, Part B Fundamentals, 28:1, 39-57, DOI: 10.1080/10407799508928820

To link to this article: https://doi.org/10.1080/10407799508928820

Published online: 25 Apr 2007.

MODIFIED COLLOCATED SIMPLEC ALGORITHM APPLIED TO BUOYANCY-AFFECTED TURBULENT FLOW USING A MULTIGRID SOLUTION PROCEDURE

Peter Johansson and Lars Davidson
Thermo- and Fluid Dynamics, Chalmers University of Technology, S-412 96 Gothenburg, Sweden

Some modifications to the collocated SIMPLEC method are presented. These modifications significantly stabilize the iteration process in buoyant flow. The modifications are made to the Rhie and Chow interpolation, the SIMPLEC iteration, and the pressure correction equation. A multigrid method is used to speed up the iteration process, and the QUICK scheme is used to approximate the convective terms. To account for turbulence we use a two-layer $k-\epsilon$ model.

INTRODUCTION

Natural-convection or temperature-driven flow is an interesting field with a large number of applications. It is thus of great interest to simulate this phenomenon in a numerical procedure. Much work has been performed over the past two decades, often using SIMPLE procedures with a staggered grid arrangement [1].

For buoyant flow, the collocated storage arrangement has had stability problems, which were reported by Vasić and Hanjalić [2] and seen in the code CALC-BFC [3]. However, the staggered arrangement is difficult to achieve for curvilinear structured meshes and even more difficult for unstructured grids. It is therefore desirable to use the more general collocated arrangement.

The major problem with natural convection is the coupling between the temperature equation and the W equation (W is the velocity component in the vertical direction). This easily gives rise to a growth of spurious error modes. Therefore buoyancy-affected flows require a much better pressure–velocity coupling than isothermal flows do. The staggered grid arrangement automatically provides a good coupling owing to the short stencil approximation of the pressure gradient and the straightforward derivation of the pressure correction equation. The collocated arrangement has a long stencil approximation of the pressure gradient, however, which allows the "checkerboard pressure mode" to grow. To

Received 23 September 1994; accepted 30 January 1995.
The support of the Swedish Research Council for Engineering Sciences (TFR) is gratefully acknowledged.
Address correspondence to Peter Johansson, Thermo- and Fluid Dynamics, Chalmers University of Technology, S-412 96 Gothenburg, Sweden.

Numerical Heat Transfer, Part B, 28:39–57, 1995

1040–7790/95 $10.00 + .00

NOMENCLATURE

a	coefficient in the discretized equation	μ	dynamic viscosity
		μ_t	turbulent dynamic viscosity
A	area of a control volume face	ν	kinematic viscosity
g	gravitational acceleration	ρ	density
h	mesh parameter	ρ_0	reference density
J	flux vector	τ_w	wall shear stress
k	turbulent kinetic energy	Φ	dependent variable
$\dot{m}$	mass flux	∇	gradient operator
n	normal distance from a wall	∇_s	short stencil approximation of a gradient operator over a control volume face
n	outward normal of a control volume face		
n^+	nu_*/ν	∇_l	long stencil approximation of a nodal gradient operator
Nu	Nusselt number		
P	pressure		
r	residual (or defect)		
Ra	Rayleigh number	**Subscripts**	
Re	Reynolds number		
S	source term in each transport equation	e, w, n, s, h, l	east, west, north, south, high, low face of a control volume
s	source term in the discretized equation	f	arbitrary face
		nb	arbitrary neighbour
T	temperature	p, E, W, N, S, H, L	center, east, west, north, south, high, low control volume
u_*	friction velocity $(\tau_\omega/\rho)^{0.5}$		
U	velocity vector		
V	volume of a control volume		
α	velocity underrelaxation parameter	**Superscripts**	
α_ρ	pressure underrelaxation parameter	ur	underrelaxed quantity
		*	old approximation
Γ	diffusion coefficient	'	correction
ϵ	dissipation of turbulent kinetic energy	$\bar{}$	linear average

suppress that pressure mode, an artificial pressure term is added to the continuity equation and Navier-Stokes equations, via a so-called Rhie and Chow interpolation [4–7].

The specific details of the construction of this term and the pressure correction equation can be very important for complex flow situations. In the present work, a modification of the standard Rhie and Chow procedure to increase the stability of the iteration process is presented. Also given are some modifications of the pressure correction equation and the SIMPLE algorithm to increase the stability.

In buoyancy-driven flow, it is of paramount importance to resolve the flow near hot and/or cold walls. Thus, more sophisticated near-wall models than standard wall functions must be used. Resolution of boundary layers can then easily result in cell aspect ratios between 100 and 1,000, which sometimes has given rise to stability problems. The present modifications have been shown to reduce these problems.

Resolving the boundary layers requires quite a number of nodes in these layers. Thus it is desirable for the mesh to be as coarse as possible in the remaining part of the domain in order to reduce the magnitude of the problem as much as possible. The second-order QUICK scheme [8] is therefore used, which is implemented in a deferred correction manner in order to stabilize the iteration process.

An estimate of the size of a three-dimensional computation with six resolved boundary layers is at least 100,000 nodes. This means that a rapid solution algorithm is needed. The multigrid method is a general method with asymptotic optimal convergence characteristics. However, turbulent multigrid calculations have been presented for only a few situations in which wall functions have normally been used [9–11]. In [12], multigrid calculations were performed using a two-layer low-Reynolds k–ϵ model of Chen and Patel [13]. In the present work, that multigrid method is applied to buoyancy-affected turbulent flows, which reduced the required CPU time by one order of magnitude.

BASIC EQUATIONS

Define a flux vector $\mathbf{J}$ containing both convection and diffusion as

$$\mathbf{J} = \rho \mathbf{U} \Phi - \Gamma \nabla \Phi \tag{1}$$

The conservation equations for stationary incompressible turbulent flow, using the k–ϵ model, can then be written as

$$\nabla \cdot \mathbf{J} = S \tag{2}$$

Table 1 shows the source terms and the diffusion coefficients for the different variables. A two-layer k–ϵ model turbulence model is used. The standard k–ϵ model is then adopted to the fully turbulent flow region, and near walls it is matched at a preselected grid line with a one-equation model. In the one-equation region, the k equation is solved and the turbulent length scale is prescribed using a mixing-length approach [13].

DISCRETIZATION

The code used is a multigrid buoyancy extended version of CALC-BFC [3, 14]. The basic algorithm is the finite-volume SIMPLEC algorithm of Patankar [1] in a collocated arrangement, which results in a system of matrix equations of the form

$$a_p^{ur} \Phi_p = \sum_{nb} a_{nb} \Phi_{nb} + s \tag{3}$$

Discretization of the Transport Equations

The coefficients a_{nb} contain the effects of both convection and diffusion, and the source terms contain the remaining terms. The convection for the k–ϵ

Table 1. The parameters in the general transport equation. The coefficients in the model are $C_\mu = 0.09$, $C_{\epsilon 1} = 1.44$, $C_{\epsilon 2} = 1.92$, $C_{\epsilon 3} = 1.0$, $\sigma_T = 0.9$, $\sigma_k = 1.0$, and $\sigma_\epsilon = 1.3$.

Equation	Φ	Γ	S
Continuity	1	0	0
Momentum	U	$\mu + \mu_t$	$-\dfrac{\partial p}{\partial x}$
Momentum	V	$\mu + \mu_t$	$-\dfrac{\partial p}{\partial y}$
Momentum	W	$\mu + \mu_t$	$-\dfrac{\partial p}{\partial z} - g(\rho - \rho_0)$
Turbulent kinetic energy	k	$\dfrac{\mu + \mu_t}{\sigma_k}$	$P_k + G_k - \rho\epsilon$
Dissipation of k	ϵ	$\dfrac{\mu + \mu_t}{\sigma_\epsilon}$	$\dfrac{\epsilon[C_{\epsilon 1}(P_k + C_{\epsilon 3}G_k) - C_{\epsilon 2}\rho\epsilon]}{k}$
Temperature	T	$\dfrac{\mu}{\mathrm{Pr}} + \dfrac{\mu_t}{\sigma_T}$	

$$P_k = \mu_t \frac{\partial U_j}{\partial x_i}\left(\frac{\partial U_j}{\partial x_i} + \frac{\partial U_i}{\partial x_j}\right) \qquad G_k = -\left(\frac{\mu_t}{\sigma_T}\right) g\beta \frac{\partial T}{\partial z}$$

$$\mu_t = \frac{C_\mu \rho k^2}{\epsilon} \qquad C_{\epsilon 3} = \frac{\tanh|W|}{\max(|U|, |V|)}$$

equations is discretized with the first-order hybrid-upwind scheme. For the velocities and the temperature the convective fluxes are approximated by the quadratic upstream scheme QUICK, in which a quadratic polynomial is fitted to one node downstream and two nodes upstream. The diffusion is discretized with central differencing.

With this discretization, the convergence of the velocities and the pressure field is expected to be second-order, as the influence of the artificial viscosity in the turbulence equations is expected to be small [10].

Discretization of the $\nabla \cdot \mathbf{U} = 0$ Constraint

It is well known that a standard collocated finite-volume method has convergence problems and that a checkerboard pressure mode will deteriorate the solution. That is because of the use of a long difference stencil approximation of the pressure gradient, which gives an odd–even decoupling of the pressure.

The same phenomenon has also been seen for finite-element methods when using the same function space for the pressure and the velocities. To cure this unpleasant phenomenon, it has been shown that, for the Stokes problem, it is sufficient to replace $\nabla \cdot \mathbf{U} = 0$ by $\nabla \cdot \mathbf{U} = h^2 \Delta p$. For the Navier-Stokes, the Galerkin/least-squares method for mixed problems is sufficient to cure both problems of velocity oscillations arising from nonresolved boundary layers and of

the spurious pressure modes [15, 16]. The Galerkin/least-squares method includes a term that is similar to the pressure dissipation term, called PWIM or Rhie and Chow interpolation [7], used in finite-volume methods.

Another strategy was suggested by Brandt [17]. He proposed that if the pressure corrections are averaged, the highest pressure mode would be filtered out. This method was tested in the present work, but difficulties were experienced in making it compatible with the SIMPLE method and deformed meshes. We have therefore chosen to solve the problem of the checkerboard pressure by loosening the $\nabla \cdot \mathbf{U} = 0$ condition by a PWIM (pressure-weighted interpolation method). In the PWIM of Rhie and Chow the mass flux $\dot{m}_f$ at a face is calculated as

$$\dot{m}_f = A_f \bar{\rho}\left\{\overline{\mathbf{U}} + \alpha\overline{Va_p^{-1}\nabla_l P} - \alpha\overline{Va_p^{-1}}\nabla_s P\right\} \cdot \mathbf{n} \tag{4}$$

The different stencils are shown for a one-dimensional case in Figure 1 with $\nabla_l P_P = (P_E - P_W)/2h$ and $\nabla_s P_{f+} = (P_E - P_P)/h$. In practice, it results in the replacement of $\nabla \cdot \mathbf{U} = 0$ by $\nabla \cdot \mathbf{U} + h^q D_h(P) = 0$, where D_h is some discrete operator.

If a_p in Eq. (4) were constant and a uniform grid were used, then D_h would be the symmetric discrete approximation of $\partial^4/\partial x^4 + \partial^4/\partial y^4 + \partial^4/\partial z^4$. This is normally called dissipation, and such terms are often added to stabilize a central difference approximation of a gradient in time-marching Runge-Kutta codes [18, 19]. As the Laplacian operator, it has a regularizing behavior. However, as the a_p coefficient normally varies, we do not obtain the discrete symmetric stencil of a fourth derivative (dissipation). Thus, rather than averaging the quantity $Va_p^{-1}\nabla_l P$, a_p^{-1}, V, and $\nabla_l P$ are averaged separately. This gives the mass flux $\dot{m}_f$ at a face as

$$\dot{m}_f = A_f \bar{\rho}\left\{\overline{\mathbf{U}} + C\overline{a_p^{-1}}\,\overline{V}\left(\overline{\nabla_l P} - \nabla_s P\right)\right\} \cdot \mathbf{n} \tag{5}$$

In this way, D_h is always a dissipation, as the nonuniformity of the mesh does not significantly affect the behaviour of D_h, at least not for smooth meshes. While the scaling factor C allows a possibility for varying the amount of dissipation, we found 0.5–1.0 to be suitable, and thus we used 0.5 through all our calculations. If smaller values were used, it was possible for overshoots in the pressure in regions of strong velocity gradients to occur. By replacing α by C, our solution is obviously independent of α. Such dependency is a drawback for the old method, where small values of α reduce the amount of dissipation.

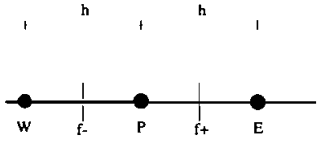

Figure 1. A one-dimensional grid.

THE SOLUTION PROCEDURE

The Full Multigrid Environment

The solution procedure is based on a multigrid environment. It reduces the amount of CPU time significantly, since the overall work of a multigrid method is linearly dependent on the size of the problem, which should be compared with the approximately quadratic dependency of the standard methods [17].

This specific multigrid method originates from a laminar multigrid [20], which was extended to turbulent flow in [12]. Here that multigrid method has been further extended to buoyant flows, via accounting for variable density.

It is a nested FMG-FAS-V-cycle approach using bilinear restriction and prolongation. The multigrid is applied to the whole equation system and uses the SIMPLEC method as a smoother. The smoothing (i.e., performing a few iterations with an iterative method) of each transport equation is performed by the TDMA. To avoid the problem of applying a Gauss-Seidel method on a nondiagonal dominant matrix, the second-order scheme QUICK is implemented in a deferred correction manner with the first-order hybrid scheme [21, 22].

In the deferred correction method the residual is assembled using the higher-order scheme, whereas the corrections are evaluated using the lower-order scheme. This is analogous to the multigrid method, where the residual is assembled on a fine mesh and the corrections are evaluated on a coarse mesh.

For more details of this specific multigrid method, see [12, 14].

SIMPLEC

The standard SIMPLEC method is described by the following steps.

1. Smooth the U, V, W momentum equations.
2. Calculate mass fluxes and smooth the pressure correction equation.
3. Smooth the k and ϵ equations.
4. Smooth the T equation.
5. Calculate the turbulent viscosity and the density (using underrelaxation).

A modification is introduced in order to more strictly enforce the $\nabla \cdot \mathbf{U} = 0$ condition during the iteration process. This is achieved by repeating step 2 four times for every iteration.

When iterating over the pressure correction equation and the evaluation of the mass fluxes, we account for the nonlinearity in the scaling of the PWIM (since we then update the a_p coefficient). We also get an influence from the ignored "long Laplacian" in the pressure correction equation. This can be viewed as a deferred correction procedure to enforce the $\nabla \cdot \mathbf{U}$ condition more strongly during each SIMPLEC iteration. This was found to stabilize the iteration process more than increasing the number of sweeps in the TDMA when smoothing the pressure correction equation. The total amount of work is not increased for either cold or hot flows, since the number of iterations is somewhat reduced.

Pressure Correction Equation

The continuity equation is transformed into a correction equation for the pressure. This is done in standard SIMPLEC by seeking a mass flux correction $\dot{m}'_f$ to the old approximation $\dot{m}^*_f$ that does not satisfy continuity, i.e.,

$$\sum_f (\dot{m}'_f + \dot{m}^*_f) = 0 \tag{6}$$

To estimate the mass flux correction $\dot{m}'_f$ we first consider a staggered control volume centered at the cell face f, where we subtract $\Sigma_{nbf} a_{nbf} U_f$ from both sides of a discrete momentum equation formed with the HYBRID scheme:

$$\frac{\overline{a_p}(1-\alpha)U_f}{\alpha} \approx \left(a^{ur}_{pf} - \sum_{nbf} a_{nbf}\right) U_f = \sum_{nbf} a_{nbf}(U_{nbf} - U_f) - V_f \nabla_s P \cdot \mathbf{n} \approx -\bar{V} \nabla_s P \cdot \mathbf{n} \tag{7}$$

where $U_f = \bar{\mathbf{U}} \cdot \mathbf{n}$. The face velocity correction U'_f is then obtained from a pressure correction field by

$$U'_f = -\frac{\alpha \bar{V}}{(1-\alpha)\overline{a_p}} \nabla_s P' \cdot \mathbf{n} \tag{8}$$

Inserted in Eq. (6) and using $\dot{m}'_f = \bar{\rho} A_f U'_f$, the standard SIMPLEC pressure correction equation reads:

$$-\sum_f \frac{\alpha \bar{\rho} \bar{V} A_f}{(1-\alpha)\overline{a_p}} \nabla_s P' \cdot \mathbf{n} = -\sum_f \dot{m}^* \tag{9}$$

After smoothing this diffusion equation by the TDMA, the pressure is updated as $p = p^* + \alpha_p p'$ and the mass fluxes by $\dot{m}_f = \dot{m}^*_f + \bar{\rho} A_f U'_f$, where U'_f is obtained from Eq. (8). A modification of this method is presented here, as the influence of the pressure dissipation correction owing to the Rhie and Chow interpolation is ignored in the standard method. When the changes in $\dot{m}_f$ by the changes in the pressure dissipation are taken into account, the continuity equation reads [see Eq. (5)]:

$$\sum_f \bar{\rho} A_f (U^*_f + U'_f) + C\overline{a_p^{-1}} \bar{V} A_f \bar{\rho} \left\{ \left(\bar{\nabla}_l - \nabla_s \right)(P^* + P') \right\} \cdot \mathbf{n} = 0 \tag{10}$$

The term $\overline{\nabla_l P'}$ is ignored for practical reasons, and the modified pressure correction equation then yields:

$$-\sum_f \bar{\rho} \bar{V} A_f \frac{\alpha + C(1-\alpha)}{\overline{a_p}(1-\alpha)} \nabla_s P' \cdot \mathbf{n} = -\sum_f \dot{m}^* \tag{11}$$

This is more or less the SIMPLE pressure correction equation with a scaling factor such as the SIMPLEC method. Equation (8) is still used to update the mass fluxes. This modification was found to contribute to only a minor stability improvement of the iteration process in buoyant flow.

RESULTS

The standard SIMPLE error measure is used, where the error for each equation is the sum of the absolute of the imbalance of each discretized equation, scaled by a characteristic flux. When all equations have a scaled error of less then 0.1%, the discrete equation system is considered convergent.

In the next subsection we discuss the improvements presented in the present work in terms of robustness for some typical problems. Then we present calculations on the square cavity $Ra = 10^6$ using the modified PWIM-SIMPLEC method to show that we have a consistent discretization. In the two last subsections we have chosen two typical cases that did not converge using the standard PWIM-SIMPLEC method.

Comparison of the Old and the Modified PWIM-SIMPLEC

We have been using the standard PWIM-SIMPLEC method successfully for 5 years, but problems occurred when we started to simulate buoyancy-driven flows. We tested at least a dozen different buoyancy-affected ventilation cases with varying amounts of temperature influence, turbulent, laminar, 2D or 3D. We could not obtain convergence in any of the turbulent calculations, except them where the buoyant effects were negligible.

For the laminar cases it was possible to obtain convergence in ventilation configurations similar to the 2D problems shown in the next subsection only if the Rayleigh number was very low.

The modifications presented stabilized the iteration process so we could achieve stationary solutions of all the above-mentioned cases. We also calculated the temperature-driven square cavity using a 40×40 grid; the old method did not converge for $Ra = 10^7$, whereas the modified method did. For $Ra \leq 10^5$ the old method had similar convergence properties as the modified one, but for $Ra = 10^6$ the old method oscillated for 300 iterations before it converged. Therefore at $Ra = 10^6$ the new method was approximately 10% faster.

We should also mention that we have yet not seen any case (cold or hot) where the old method is superior to the new one, but for flows where the old method performs well, the modifications do not seem to give any improvements either.

For the cavity flow $Ra = 10^6$ $\overline{Nu}$ was calculated using both the old and the new approaches. On the 10×10 grid the difference was 0.013, on the 20×20 grid it was 0.0013, and on the 40×40 grid the difference was 0.00018. Comparing these differences to the other numerical errors, we see that the differences in $\overline{Nu}$ due to the changes in the pressure dissipation are negligible. These differences also decay cubically compared to the quadratic convergence of the other discretization errors.

Table 2. Convergence data, mean Nusselt numbers, maximum value of the streamfunction, and its location for the laminar cavity, Ra = 10^6, compared to the benchmark solution of de Vahl Davis [24]

	WU_{FMG}	$\overline{Nu}$	$\lvert\Psi_{max}\rvert$	x_{max}	z_{max}
10 × 10	604	8.669	15.850	0.265	0.570
20 × 20	605	8.769	16.420	0.182	0.573
40 × 40	310	8.813	16.691	0.159	0.554
80 × 80	161	8.823	16.775	0.152	0.549
160 × 160	131	8.825	16.803	0.151	0.548
Benchmark		8.800	16.750	0.151	0.547
Rel. diff.		0.28%	0.31%	< 0.1%	0.18%

Since similar behavior was observed for the streamfunction, we conclude that the new and the old PWIM give the same accuracy but that the new is more robust.

Temperature-Driven Cavity, Ra = 10^6

The first application that is calculated using the new PWIM-SIMPLEC method is a square cavity with one hot vertical wall and one cold wall at the opposite side. The Rayleigh number is 10^6, which is a stable laminar case. The grid is a nonuniform 160 × 160 grid with a highest aspect ratio of 23, which has been referred to as a high value in multigrid calculations [23].

For the multigrid the number of iterations needed for convergence was independent of grid density (see Table 2). The speedup of the FMG method was 10 for the 40 × 40 grid, so it is at least 100 for the 160 × 160 grid.

The expected second-order convergence of the solution is indicated by the fact that all quantities in Table 2 converge quadratically. As can be seen in Table 2, the agreement compared to the benchmark solutions presented by G. de Vahl Davis [24] is very good. The benchmark solution has an accuracy of 1%, and our results differ by 0.3% at most from the benchmark values.

Figure 2 shows the streamline contours and contours of constant temperature for Ra = 10^6.

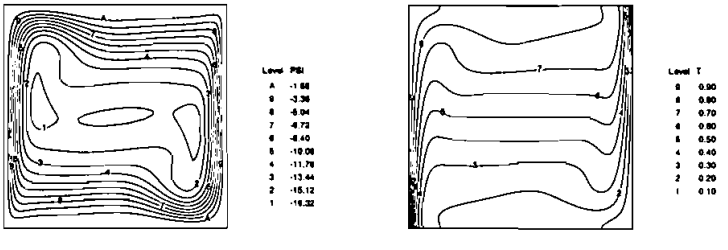

(*a*) (*b*)

Figure 2. Contours of (*a*) constant Ψ and contours of (*b*) constant T.

Two-Dimensional Ventilated Room

The next application is a two-dimensional model of a room with an inlet (with cold incoming air, $T_{in} = 0°C$) placed on the left wall under the ceiling and an outlet placed on the opposite wall close to the floor (see Figure 3.) A hot window ($T_{win} = 50°C$) is located on the outlet wall. Three different Reynolds numbers $Re = U_{in} H_{in}/\nu$ (based on the mean inlet velocity and the inlet height) were calculated: Re = 3,890; 5,170; and 6,470. The ratio between the inlet height H_{in} and the height H of the room is $H_{in}/H = 0.0080$, and the length of the room is $L = 3H$. The outlet is placed near the floor, and the outlet height is $H_{out} = 0.036 \times H$. The hot window ($H_{win} = 0.93 \times H$) is placed symmetrically between the floor and the ceiling. The Rayleigh number (based on the window height and the temperature difference between the window and the inlet jet) is $Ra = 1.2 \times 10^{11}$ for all calculations.

This is a turbulent flow problem, and the destruction term G_k is included in the low-Reynolds k–ϵ model (see Table 1). As the vertical temperature gradient is chiefly negative ($\partial T/\partial z < 0$), the G_k term is primarily negative. This reduces the turbulent viscosity, a fact that destabilizes the equation system. A high resolution is needed at walls, especially at the hot wall. Thus a 160×80 mesh with a highest aspect ratio of 2,240 near the horizontal walls and 1,770 near the vertical walls was used, which gives the necessary resolution (for the nodes adjacent to the wall, $n^+ < 0.5$). The resolution is also sufficient in the remaining part of the room, as only very small visible changes of the flow could be seen when an 80×40 grid was used instead of a 160×80 grid. For $Ra = 10^{11}$, Henkes [25] calculated the cavity transiently with a low-Reynolds k–ϵ model. He showed that the unstationarity dies out, although this requires at least 1,000 time steps using the HYBRID scheme and a staggered grid arrangement. Others have reported that the unstationarity does not die out [26].

It is therefore appropriate to suspect that there is a strong unstationarity originating from the W–T coupling, and which is only slowly damped out (or not damped) by the turbulence model. When solving the steady equations, this unstationarity would probably destroy the convergence. This might be the reason for the problems with the standard PWIM-SIMPLEC method in [3]. Even though it was significantly stabilized with the modifications made in the present work, it is still more difficult to achieve steady solutions in buoyant flows than in isothermal flows.

The three cases are calculated with the multigrid method, which shows good performance. The estimated speedup is of the order of 10 times. The drawback is that, in spite of the use of a four-level multigrid, the flow case where Re = 6,470 required 1,500 iterations, the case where Re = 5,170 required 2,500 iterations, and the case where Re = 3,890 required 15,000 iterations. The great number of

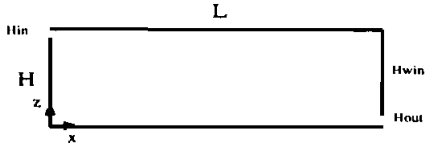

Figure 3. The two-dimensional ventilated room configuration.

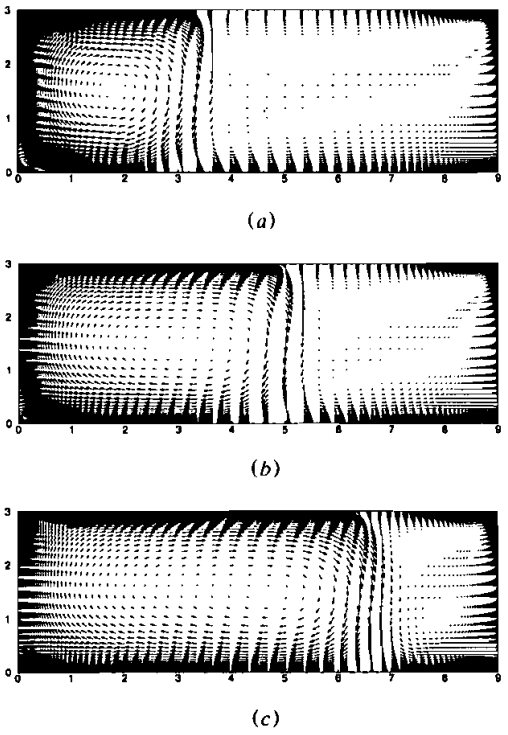

Figure 4. Velocity vector plots for the two-dimensional ventilated room with Re = (*a*) 3,890; (*b*) 5,170; and (*c*) 6,470.

iterations as compared with the laminar flow and the isothermal turbulent flow was the result of having to use stricter underrelaxation and a more stable V cycle in order to obtain convergence. The difference between the first two calculations and the last one is that it was necessary to underrelax the last more strictly. The single-grid calculation at the coarsest mesh (20 × 10) does not converge within less than 1,000–5,000 iterations, depending on the case, and thus the multigrid still retains most of the property of not using more iterations on a fine grid than on a coarse grid. However, the convergence history is not monotonous, and may diverge for 100 iterations and then continue to converge again. Having established these convergence problems, we must remember that for these flows the old method did not converge at all.

Figure 4 shows the velocity vector plots, and Figure 5 shows contours of constant temperature. As all boundaries except the inlet and the window are adiabatic, the constant-temperature contours are orthogonal to these surfaces for the 5–10 nodes adjacent to the boundary. This cannot be seen in Figure 5 because the boundary layers are very thin. Figure 6 shows that the boundary layers are well resolved. The high resolution is also seen in Figure 7, wherein the secondary eddy and third eddy in the lower-left corner of the room for Re = 3,890 are shown.

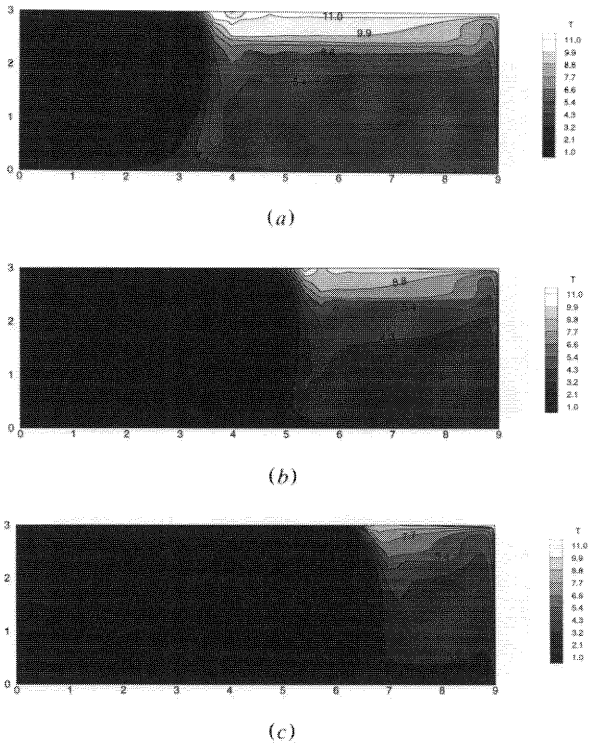

Figure 5. Contour of constant-temperature plots for the two-dimensional ventilated room with Re = (*a*) 3,890; (*b*) 5,170; and (*c*) 6,470.

Three-Dimensional Ventilated Room

This case was investigated both experimentally and numerically in an IEA project called ANNEX 20 [27]. Here we study case E1, and the configuration is shown in Figure 8. It is a room with a height $H = 2.5$ m, a width $B = 3.6$ m, and a length $L = 4.2$ m.

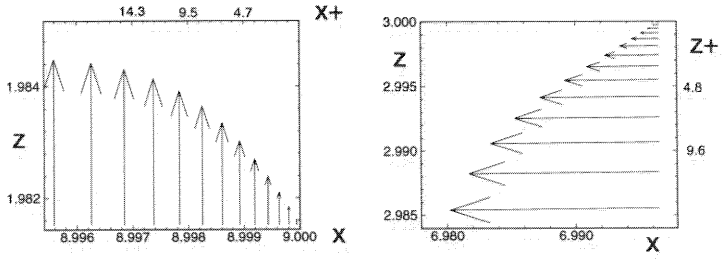

Figure 6. Vector plots showing the boundary layers at the hot wall and at the ceiling in the two-dimensional ventilated room.

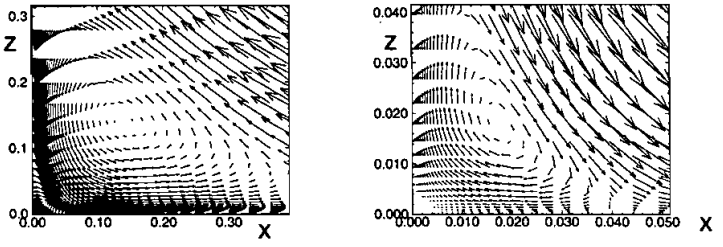

Figure 7. Vector plot of the "secondary" and the "third" eddy in the "low-west" corner.

On the front wall, an inlet with 84 nozzles is placed 0.285 m below the ceiling symmetrically between the side walls. The nozzles are inclined 40° toward the ceiling. On the front wall, an outlet (H_{out} = 0.2 m and B_{out} = 0.3 m is placed 1.7 m from the floor and symmetrically between the side walls. On the opposite wall, a window (H_{win} = 1.6 m and B_{win} = 2.0 m) is symmetrically located 0.7 m above the floor. The inlet diffuser in the calculations is represented by a small rectangular inlet (H_{in} = 0.062 m and B_{in} = 0.18 m) to obtain the equivalent mass and momentum fluxes. The volume flux of the jet is $\dot{V}$ = 0.0158 m^3/s, the inlet temperature T_{in} = 10°C, and the window temperature T_{win} = 30°C. The walls have a constant temperature of 21°C, except for the front wall, which has a temperature of 22°C. The inlet boundary conditions of the turbulence kinetic energy and the dissipation of turbulent kinetic energy are set as $k_{in} = 0.01 \times (U^2 + W^2)$ and $\epsilon_{in} = 0.00016 \times (U^2 + W^2)\ 1.5/d_h$, where d_h is the hydraulic diameter.

At the outlet, a constant velocity U_{out} is specified and a symmetry condition is used for the remaining variables. This is a very difficult flow case to simulate [27], as the cold inlet jet should drop and hit the floor before it has reached the opposite wall. It has low physical stability because small disturbances of the inlet jet will cause a great effect in the region where the jet drops toward the floor. Note that although the geometry and the boundary conditions are symmetric with respect to the vertical plane $y = B/2$, the flow is not symmetric, neither in the experiments nor in the predictions.

The grid used is a stretched 56 × 56 × 56 grid and has a highest cell aspect ratio of over 500. The high stretching gives the necessary resolution of the boundary layers, i.e., $n^+ < 0.5$ at the node adjacent to the hot window. Grid lines

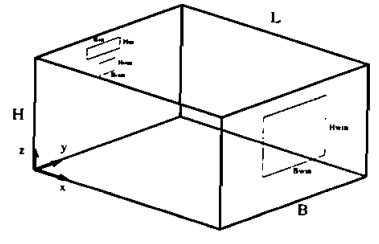

Figure 8. The three-dimensional ventilated room configuration: ANNEX20 E1.

are also concentrated in the region of the inlet jet and the outlet. The difference between the solution obtained on a $28 \times 28 \times 28$ grid and that on a $56 \times 56 \times 56$ grid is not significant. In fact, the major structures of the flow are resolved on a $14 \times 14 \times 14$ grid. This is possible because the QUICK scheme is used to approximate the convective fluxes for the velocities and the temperature, and because the grid is highly stretched near the walls. Thus the solution on the fine grid is believed to be a grid-independent solution (the model errors are larger than the numerical errors). One model error is introduced by the turbulence model, and another is the approximation of the inlet, where the 84 nozzles were replaced by a single jet.

For the same reasons as in the two-dimensional turbulent case, it is difficult to achieve stationary solutions in three dimensions. While this was noted, it was possible to obtain a stationary solution within 2,500 WU with a three-level multigrid cycle with a convergence criterion 1% instead of the 0.1% used earlier. This is the same number of iterations needed to achieve a solution on the coarsest grid, which means that the multigrid retains its asymptotic properties. When the convergence criterion was set lower, the convergence stagnated and a restart with stricter underrelaxation parameters was necessary to obtain further convergence.

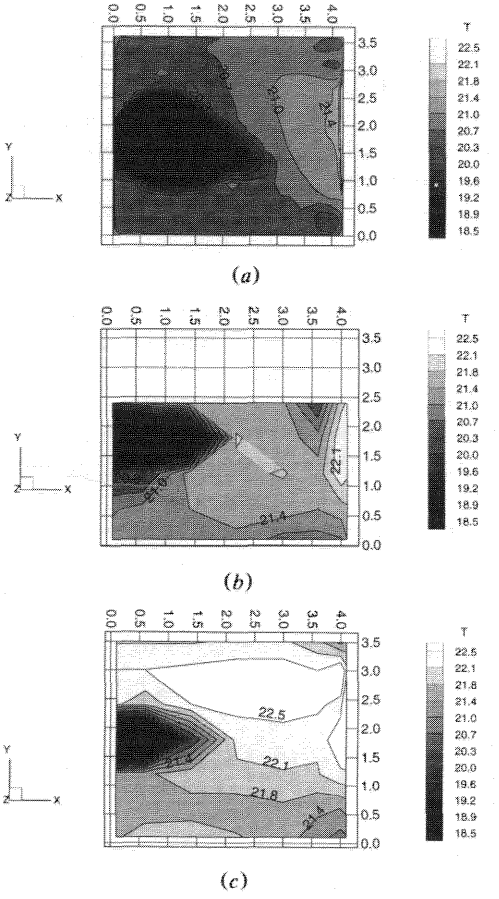

Figure 9. Contours of constant temperature for the three-dimensional ventilated room, $z = 2.45$ m (horizontal plane, seen from above). (*a*) predictions; (*b*) measurements by Fossdal; (*c*) measurements by Blomkvist.

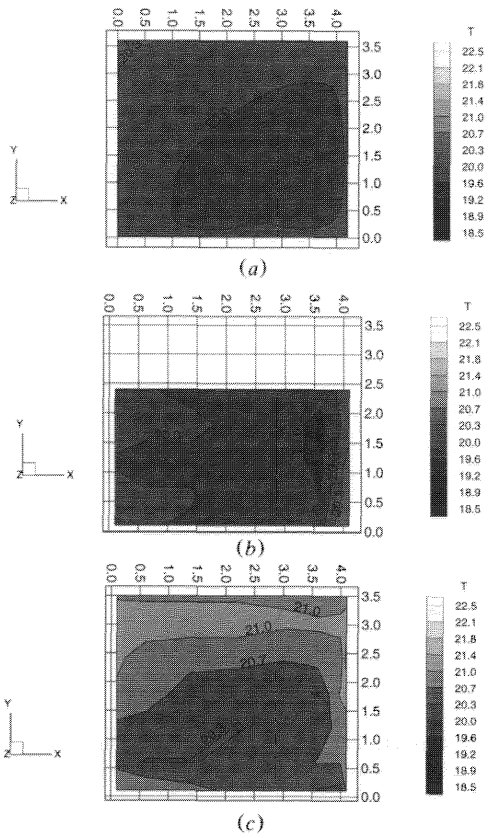

Figure 10. Contours of constant temperature for the three-dimensional ventilated room, $z = 0.05$ m. See legend in Figure 10.

Another alternative was to restart transiently and use the V cycle at each time step and then let the unstationarity die out. That was shown to be somewhat faster than using stricter underrelaxations. However, both methods need about 2,000–5,000 WU to reduce this last magnitude of the residual error, which is of academic interest for this specific case, as the solution was not notably changed between a residual error of 10% and one of 1%. Note that to start from a zero initial guess and solve this transiently until a steady solution is obtained requires a very large amount of work. In the $14 \times 14 \times 14$ case, it required at least 25 times as much work in comparison with using the stationary equations.

The predictions are compared with two different measurements [28, 29]. Figures 9 and 10 compare the calculated temperature field with the measured ones in two different slices of the domain. In Figure 11 the calculated inlet region is zoomed. In Figure 12 the entrainment of air into the jet, which creates two longitudinal vortices, is shown. In Figure 12 we can also see the deflection of the cold jet while it is falling toward the floor. Close to the ceiling in the middle of the x–y plane, the cold inlet jet meets the warm flow from the hot window. The inlet jet is then deflected toward the "low-y" wall while falling toward the floor. This jet

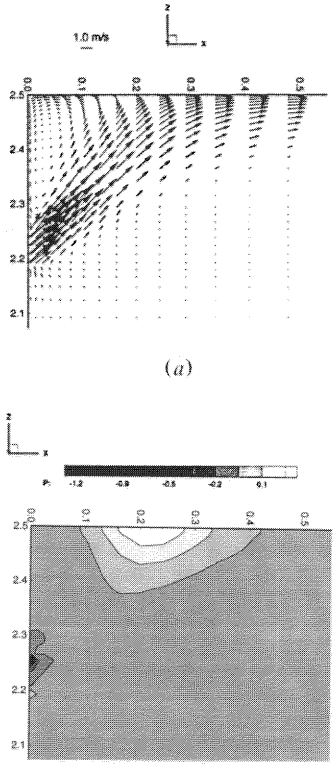

Figure 11. The inlet region at $y = 1.8$ m, velocity vectors (*a*), constant contours of pressure (*b*).

then hits the floor before it has reached the "high-x" wall (see Figures 10 and 12). The calculations and Fossdal's [28] measurements are in good agreement, and the jet hits the floor at $x/L = 0.8$, $y/B = 0.4$ in both cases, whereas in Blomkvist's [29] measurement the jet hits the floor at $x/L = 0.4$, $y/B = 0.25$ (see Figure 11).

At the ceiling (Figure 9), our simulation and Fossdal's measurements show an attachment region of the inlet jet of similar size, whereas Blomkvist shows a quite smaller attachment region. However, the calculations predict a deflection at the ceiling of the inlet jet, whereas in the measurements the deflection occurs when the jet is falling toward the floor. That may be an effect of the modeling of the inlet.

Overall, the calculations are in better agreement with the measurements made by Fossdal than with those of Blomkvist. In general, Blomkvist's temperatures are 1°C higher than those measured by Fossdal and in the present calculations.

In general, the difference between the calculations and the measurements is not larger than the difference between the two measurements. (For a more detailed comparison, see [14].)

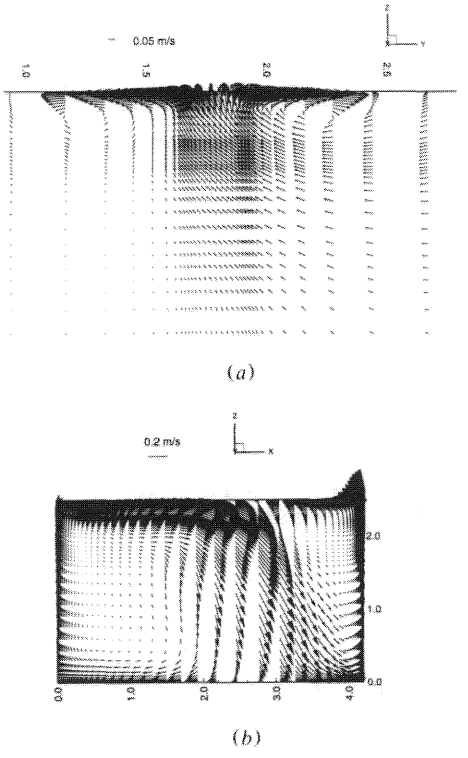

Figure 12. Velocity vectors at $x = 0.4$ m (*a*), $y = 1.2$ m (*b*).

CONCLUSION

Three modifications of a collocated SIMPLEC method are introduced:

1. One scaling in the Rhie and Chow interpolation is used instead of the usual three. This ensures that a symmetric discretization of a fourth derivative is achieved.
2. In order to enforce the continuity constraint more strictly during the iteration process, we make a loop over the calculation of mass fluxes and the pressure correction equation.
3. The coefficients in the pressure correction equation are modified with respect to the pressure dissipation.

The modifications were found to stabilize the iteration process for buoyant flows significantly.

The multigrid method applied to buoyant flow retained most of its asymptotic behavior and reduced the required CPU time by a magnitude.

The buoyancy-affected flow in a three-dimensional room was predicted within the spreading of the measurement sets.

REFERENCES

1. S. V. Patankar, *Numerical Heat Transfer and Fluid Flow,* Hemisphere, New York, 1980.
2. S. Vasić and K. Hanjalić, Turbulent Natural Convection in a Square Cavity, in *Turbulent Natural Convection in Enclosures,* pp. 133–144, Editions Européennes Thermique et Industrie, Paris, France, 1993.
3. L. Davidson and B. Farhanieh, A Finite Volume Code Employing Collocated Variable Arrangement and Cartesian Velocity Components of Fluid Flow and Heat Transfer in Complex Three-Dimensional Geometries, Department of Thermo- and Fluid Dynamics Rept. 91/14, Chalmers University of Technology, Gothenburg, Sweden, 1991.
4. S. K. Choi, H. Y. Nam, and M. Cho, Use of the Momentum Interpolation Method for Numerical Solution of Incompressible Flows in Complex Geometries: Choosing Cell Face Velocities, *Numer. Heat Transfer B,* vol. 23, pp. 21–41, 1993.
5. S. Majumdar, W. Rodi, and S. P. Vanka, On the Use of Non-staggered Pressure–Velocity Arrangement for Numerical Solution of Incompressible Flows, Rept. SFB 210/T/35, Sonderforschungsbereich, Universität Karlsruhe, Karlsruhe, Germany, 1987.
6. M. Perić, R. Kessler, and G. Scheuerer, Comparison of Finite-Volume Numerical Methods with Staggered and Collocated Grids, *Computers and Fluids,* vol. 16, no. 4, pp. 389–403, 1988.
7. C. M. Rhie and W. L. Chow, Numerical Study of the Turbulent Flow Past an Airfoil with Trailing Edge Separation, *AIAA J.,* vol. 21, pp. 1525–1532, 1983.
8. B. P. Leonard, A Stable and Accurate Convective Modeling Procedure Based on Quadratic Upstream Interpolation, *Comp. Meth. Appl. Eng.,* vol. 19, pp. 59–98, 1979.
9. Y. Li, L. Fuchs, and S. Holmberg, An Evaluation of a Computer Code for Predicting Indoor Airflow and Heat Transfer, *12th AIVC Conf.,* Ottawa, Canada, pp. 123–136, 1991.
10. F. S. Lien, Computational Modelling of 3D Flow in Complex Ducts and Passages, Ph.D. thesis, University of Manchester, Manchester, England, 1992.
11. M. Perić, M. Rüger, and G. Scheuerer, A Finite Volume Multigrid Method for Calculating Turbulent Flows, *Proc. 7th Symp. on Turbulent Shear Flows,* Stanford, CA, pp. 7.3.1–7.3.6, 1989.
12. P. Johansson and L. Davidson, A Full Multigrid Method Applied to Turbulent Flow Using the SIMPLEC Algorithm Together with a Collocated Arrangement, in *Multigrid Methods IV,* pp. 245–256, Birkhäuser Verlag, Basel, Switzerland, 1994.
13. H. C. Chen and V. C. Patel, Near-Wall Turbulence Models for Complex Flows Including Separation, *AIAA J.,* vol. 26, pp. 641–650, 1988.
14. P. Johansson, Numerical Simulations of Three-Dimensional Ventilated Enclosures Using a Full Multigrid Method, Thesis for the degree of Licenciate of Engineering Department of Thermo- and Fluid Dynamics, Rept. 94/4, Chalmers University of Technology, Gothenburg, Sweden, 1994.
15. M. Behr and T. E. Tezduyar, Finite Element Solution Strategies for Large-Scale Flow Simulations, *Comp. Meth. Appl. Mech. Eng.,* vol. 112, pp. 3–24, 1994.
16. P. Hansbo and A. Szepessy, A Velocity-Pressure Streamline Diffusion Finite Element Method for the Incompressible Navier-Stokes Equations, *Comp. Meth. Appl. Mech. Eng.,* vol. 84, pp. 175–192, 1990.
17. A. Brandt, Multigrid Techniques: 1984 Guide with Applications to Fluid Dynamics, Computational Fluid Dynamics Lecture Notes at Von-Karman Institute, Brussels, Belgium, 1984.
18. A. Jameson, W. Schmidt, and E. Turkel, Numerical Solutions of the Euler Equations by Finite Volume Methods with Runge-Kutta Time-Stepping Schemes, AIAA Paper 81-1259, 1981.
19. A. Rizzi, Damped Euler-Equation Method to Compute Transonic Flow around Wing-Body Combinations, *AIAA J.,* vol. 20, pp. 1321–1328, 1982.

20. P. Johansson, A Three-Dimensional Laminar Multigrid Method Applied to the SIMPLEC Algorithm, Diploma thesis, Department of Thermo- and Fluid Dynamics, Rept. 92/5, Chalmers University of Technology, Gothenburg, Sweden, 1992.
21. S. C. Caruso, J. H. Ferziger, and J. Oliger, Adaptive Grid Techniques for Elliptic Fluid-Flow Problems, Thermosciences Division, Department of Mechanical Engineering, Rept. TF-23, Stanford University, Stanford, CA, 1985.
22. M. C. Thompson and J. H. Ferziger, An Adaptive Multigrid Technique for the Incompressible Navier-Stokes Equations, *Int. J. Comp. Phys.*, vol. 82, no. 1, pp. 94–121, 1989.
23. P. M. Sockol, Multigrid Solutions of the Navier-Stokes Equations on Highly Stretched Grids, *Int. J. Numer. Meth. Fluids,* vol. 17, pp. 543–566, 1993.
24. G. de Vahl Davis, Natural Convection in a Square Cavity: A Bench Mark Numerical Solution, *Int. J. Numer. Meth. Fluids,* vol. 3, pp. 249–264, 1983.
25. R. A. W. M. Henkes, Natural-Convection Boundary Layers, Ph.D. thesis, Delft University, Delft, The Netherlands, 1990.
26. H. Ozoe, M. Mouri, Ohmuro, S. W. Churchill, and N. Lior, Numerical Calculation of Laminar and Turbulent Natural Convection in Water in Rectangular Channels Heated and Cooled Isothermally on the Opposing Vertical Walls, *Int. J. Heat Mass Transfer,* vol. 28, pp. 125–138, 1985.
27. ANNEX 20, Room Air and Flow Contaminant Flow, Evaluation of Computational Methods, Subtask 1, Summary Report, A. D. Lemaire (ed.), TNO Building and Construction Research, Delft, The Netherlands, 1993.
28. S. Fossdal, Measurement of Test Case E (Mixed Convection, Summer Cooling), IEA ANNEX 20, Research Item 1.17, Pre. Rept. NBRI, Oslo, Norway, 1990.
29. C. Blomkvist, Measurement of Test Case E (Mixed Convection, Summer Cooling), IEA ANNEX 20, Research Item 1.17, Tech. Rept. NSIBR, Gävle, Sweden, 1991.